Bulletin of the Seismological Society of America, Vol. 95, No. 2, pp. 431–445, April 2005, doi: 10.1785/0120040052

The 6 June 2003 Bardwell, Kentucky, Earthquake Sequence: Evidence for a Locally Perturbed Stress Field in the Mississippi Embayment

by Stephen P. Horton, Won-Young Kim, and Mitch Withers

Abstract This article describes an unusually well-behaved, unusually well-documented central and eastern United States (CEUS) earthquake sequence. Detailed analysis of regional and local waveform data from the 6 June 2003 Bardwell, Kentucky, earthquake indicates that the mainshock has the seismic moment of M_0 1.3 ($\pm$0.5) $\times$ 10^{15} N m (M_w 4.0) and occurred at a depth of about 2 ($\pm$1) km on a near-vertical fault plane. A temporary seismic network recorded 85 aftershocks that delineate an east-trending fault approximately 1 km in length. The hypocenters illuminate a vertical plane between 2.0 and 2.7 km depth. The centroid of the aftershock distribution is at 36.875° N, 89.010° W and a depth of 2.4 km. The aftershock cluster is interpreted as a circular fault area with a radius of 0.44 ($\pm$0.03) km. This source radius yields a static stress drop, $\Delta\sigma = 67$ ($\pm$14) bars for the mainshock. The focal mechanism for the mainshock has strike = 90°, dip = 89°, and rake = $-165°$ with a subhorizontal P axis trending 135°. A formal stress inversion based on the focal mechanisms of the mainshock and ten aftershocks indicates the maximum compressive stress trends 104° with a plunge of 5°. The local stress field near Bardwell is therefore rotated about 40° clockwise relative to 65° for eastern North America as a whole. The Bardwell earthquakes have the opposite sense of slip to earthquakes with east-trending nodal planes that occur near New Madrid, Missouri. This requires a significant local rotation of the stress field over a distance of 60 km.

Introduction

On 6 June 2003 at 12:29 (UTC), a moderate-sized (M_w 4) earthquake occurred near Bardwell, Kentucky (Fig. 1). Bardwell is approximately 57 km northeast of New Madrid, Missouri, in an area of transition from the northeast-trending Reelfoot rift to the east-trending Rough Creek graben. The Bardwell mainshock was felt in western Kentucky and parts of Tennessee, Missouri, and Indiana. Ground acceleration recorded in Wickliffe, Kentucky, approximately 13 km from the epicenter, attained a peak of 0.02g (Wang *et al.*, 2003). Minor damage was reported in and around the town of Bardwell. Bricks fell from a two-story masonry building in the center of town. An archway in the courthouse sustained cracks in the mortar and some broken bricks. A portion of the ceiling collapsed in the local Dollar General Store. Several residents of Bardwell reported that a loud explosive sound preceded strong shaking. A county judge heard a "low rumble" turn into a "deafening roar" right before the earthquake hit. The shaking was strong enough to encourage some residents to exit their houses and to cause some difficulty in standing.

Within 15 hr after the mainshock, a temporary network of five broadband seismographs had been installed in the epicentral area to record aftershocks. Although an M_w 4 earthquake is rather small to warrant the effort for an aftershock study, this is one of the two largest earthquakes to occur in the Mississippi embayment since the upgrade of the regional seismic network beginning in 1998. A four-week-long aftershock survey captured 85 aftershocks that produced high-quality three-component broadband seismic records. The aftershocks are tightly clustered and have magnitudes up to 2.4. Thus, the mainshock and aftershocks provide data for the study of seismic wave propagation in deep soils and tectonic processes in an intraplate region. In this article, we characterize seismic sources and the local stress field.

A primary goal of the aftershock study is to determine the depth and fault geometry of the mainshock. The distribution of aftershocks derived from a standard single-event location method clearly defines an east-trending fault plane about 1 km in length and about 2.5 km underneath the town of Bardwell. However, the significance of the inferred fault geometry is diminished because the location uncertainties are on the same order as the fault dimensions. To reduce the level of location uncertainty, we applied the double-difference earthquake location method (Waldhauser, 2001). As in the Aftershock Location section, the double-difference method

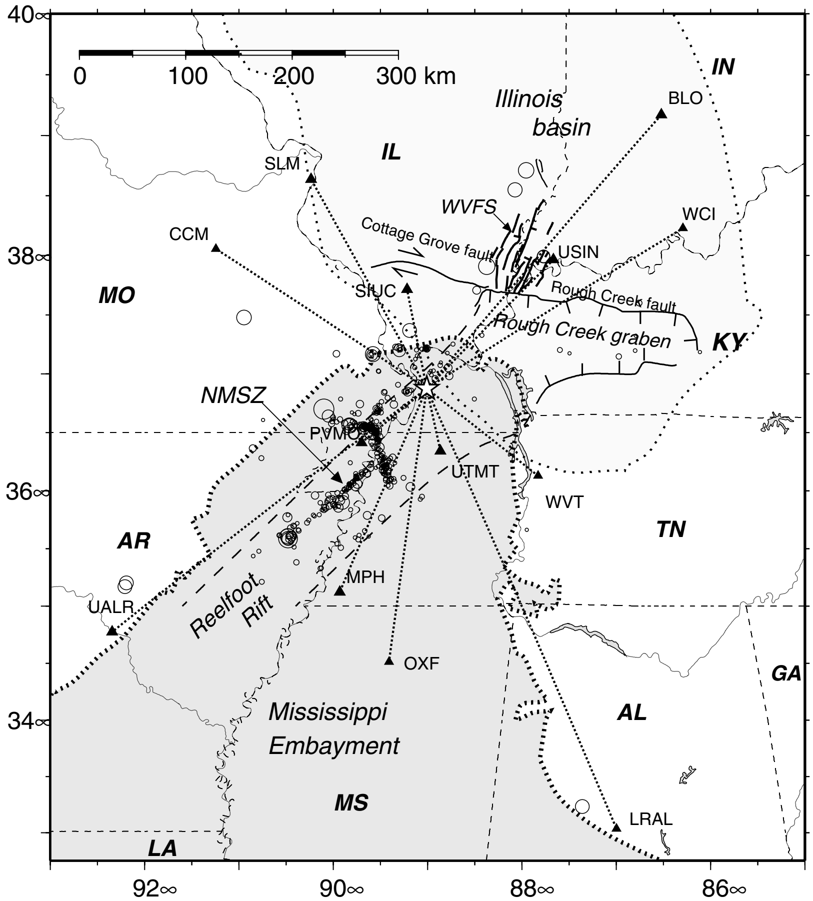

Figure 1. Major geologic features around the epicentral area, the Mississippi embayment and Illinois basin, are indicated by the shaded areas. The epicenter of the 6 June 2003 Bardwell, Kentucky, earthquake is plotted with a star. Heavy dashed lines indicate the Reelfoot rift, a failed rift system in the northern Mississippi embayment. The Rough Creek graben in western Kentucky, the Rough Creek fault, and Wabash Valley fault system (WVFS) along southeastern Illinois-southwestern Indiana border are indicated by solid lines with tics on downthrown sides. Earthquakes with $m_{bLg} \geq$ 2.5 in the New Madrid seismic zone (NMSZ) and events with $m_{bLg} \geq$ 4.5 that occurred in other areas during 1960–2002 are plotted for reference (Central Mississippi Valley Earthquake catalog, 1975–1994, St. Louis University; Gordon, 1988; Preliminary Determination of Epicenter [PDE] monthly listing). Modern broadband seismographic stations are plotted with solid triangles, and source-receiver paths are indicated by dotted lines.

promotes an order-of-magnitude improvement in uncertainty compared with single-event locations (Waldhauser and Ellsworth, 2000). After relocation, the mainshock fault geometry is determined with increased confidence. A fault radius is estimated and, along with the seismic moment, is used to estimate the static stress drop for the mainshock.

A second goal of the aftershock study is to obtain an estimate of the orientation of the local stress field indicated by the mainshock and aftershocks of the Bardwell earthquake sequence. The focal mechanism of the mainshock is determined, and we obtained well-constrained focal mechanisms for ten aftershocks by using *P*-, *SH*-, and *SV*-wave polarities and amplitude ratios of these phases. These focal mechanisms are the basis for a stress tensor inversion using the method developed by Gephart (1990).

Tectonic Setting

The 2003 Bardwell earthquake sequence occurs in the northern Mississippi embayment (Fig. 1), a southwest-plunging synclinal trough of poorly consolidated to unconsolidated sediments (Stearns, 1957). The synclinal axis roughly coincides with the present course of the Mississippi River. The Late Cretaceous to Recent clastic sediments are about 340 m thick in the study area, thicken to about 1000 m near station MPH (Fig. 1), and feather erosionally to zero thickness at the embayment margins (Dart, 1992). These sediments lie unconformably atop Paleozoic sedimentary rock. The Paleozoic rocks form a veneer several kilometers thick lying unconformably above the crystalline basement. The Precambrian basement is found at 4200 m depth in the Dow Chemical no. 1 Wilson drill hole (Howe, 1984) in southeastern Arkansas. The crystalline basement is part of a vast Proterozoic (1.48–1.45 Ga) igneous province stretching from northern Mexico to eastern Quebec termed the "eastern granite-rhyolite province" (Bickford *et al.*, 1986).

The structural framework of the study area is complex. The embayment sediments have a regional dip toward the south and toward the axis of the embayment trough (Stearns, 1957). However, the underlying Paleozoic rocks in the study area dip northeast toward the Illinois basin and away from the Ozark uplift and Pascola arch (Kolata *et al.*, 1981). Precambrian basement outcrops in the St. Francis Mountains of the Ozark uplift, but the top of the Precambrian basement deepens progressively toward the Illinois basin (McBride *et al.*, 2003). The top of the Precambrian basement is between 3 and 4 km deep in the study area, and 7 to 9 km deep near the Rough Creek fault (Bertagne and Leissing, 1991; Wheeler *et al.*, 1997).

Two large rifts in the Precambrian basement occur in the study area: the Reelfoot rift and the Rough Creek graben. The northeast-trending Reelfoot rift formed during a platewide extensional event in the early Cambrian (Burke and Dewey, 1973) and reactivated during the Cretaceous to form the Mississippi embayment (Ervin and McGinnis, 1975). Gravity and magnetic anomalies are interpreted as a northeast-trending graben 70 km in width and more than 300 km in length with structural relief of about 2 km (Hildenbrand *et al.*, 1977, 1982; Kane *et al.*, 1981). The maximum depth to basement is about 5 km in the center of the rift and 3 km at the flanks (Kane *et al.*, 1981; Ginzburg *et al.*, 1983; Mooney *et al.*, 1983; Hildenbrand, 1985). The Reelfoot rift may be underlain by a rift pillow, a high-velocity and high-density crustal layer 30–40 km deep (Ginzburg *et al.*, 1983; Mooney *et al.* 1983). The east-trending Rough Creek graben is approximately the same age as and contiguous with the Reelfoot rift (Kolata and Hildenbrand, 1997).

The New Madrid Seismic Zone (NMSZ) southwest of Bardwell in Figure 1 is in the Reelfoot rift. Concentrated microseismic activity delineates two northeast-trending segments offset by a north-northwest-trending segment. In the southern segment, earthquakes are concentrated along the center of the Reelfoot rift axis. The Reelfoot rift is the most seismically active of six Iapetan rifts and grabens in central and eastern North America, whereas the Rough Creek graben is one of the least active (Wheeler *et al.*, 1997).

Three large earthquakes occurred in the NMSZ during the winter of 1811–1812. Paleoliquifaction evidence suggests five to nine magnitude 7–8 earthquakes have occurred in the NMSZ in the past 1100 years (Tuttle *et al.*, 2002). Global positioning satellite observations indicate differential displacement rates less than 1–2 mm/yr (Newman *et al.*, 1999; Santillan *et al.*, 2002). The three largest earthquakes in the NMSZ since the regional seismic network was established in 1974 are the 25 March 1976, Marked Tree, Arkansas, earthquake (mb(Lg) = 5.0; Herrmann, 1979); 26 September 1990, Cape Girardeau, Missouri, earthquake (mb(Lg) = 4.7; Langston, 1994); and the 4 May 1991, Risco, Missouri, earthquake (mg(Lg) = 4.6; Langston, 1994). These and other earthquakes that occurred in the NSMZ are predominantly strike-slip faulting on steeply dipping nodal planes with subhorizontal *P* axes trending east-northeast–east (see Table 1).

As opposed to the well-defined seismicity patterns of the NMSZ, seismicity to the north in southern Illinois and Indiana is more dispersed. The largest instrumentally recorded earthquake in the region is the 9 November 1968, southern Illinois earthquake (M_w 5.3; Table 1). Munson *et al.* (1997) found paleoliquifaction evidence in the southern halves of Illinois and Indiana for at least six large (M_w > 6.0) Holocene earthquakes.

Since the Late Cretaceous (70 Ma) to present, east–west-trending horizontal compressive stress has been the primary tectonic force in the epicentral region (Kolata and Nelson, 1991). This regional stress may reactivate faults in the crystalline basement within the Reelfoot rift and the surrounding area.

Mainshock Focal Mechanism and Depth from Waveform Inversion

The 6 June 2003, Bardwell, Kentucky, earthquake was well recorded by broadband seismographic stations in the central and eastern United States (Fig. 1). Regional seismic records at 13 stations in the distance range from 59 to 463 km are used to determine the focal mechanism and depth. The observed records are modeled using a frequency-wavenumber (*f-k*) integration method for a point source embedded in a simple 1D crustal velocity model (Saikia, 1994). A central United States crustal model with four layers over a half-space is used (Herrmann, 1979). A grid-search waveform inversion technique (Zhao and Helmberger, 1994) is used. This method matches observed seismograms against synthetics over discrete wave trains and allows relative time shifts between individual wave trains. The preferred solution minimizes the fitting error in terms of four source parameters: seismic moment (M_0), strike, dip, and rake (see Kim, 2003). A global minimum error is sought for a range of trial depths.

A common problem in modeling regional waves is inadequate knowledge of the crustal structure and the corresponding Green's functions. One approach is to remove high-frequency body waves and model only the long-period surface waves at about 20 sec period, as discussed by Zhao and Helmberger (1994) and Tio and Kanamori (1995). We model the complete waveform including body waves and surface waves over the period range from 8 to 20 sec for records at distances less than 200 km, and from 10 to 30 sec for records at greater distances. The filtered records are dominated by fundamental mode Rayleigh and Love waves but also include *Pnl* waves. The *P*-wave first-motion data from eight stations are also added in the inversion to help constrain the source mechanism. The inversion for focal mechanism parameters is carried out as a grid search through the whole parameter space of strike, dip, and rake.

Figure 2 shows the comparison between the observed and synthetic waveforms for the best-fit solution. The observed signals are very well matched by the synthetics. The time shifts (δt) required to align the 32 traces are mostly positive with an average of 0.9 sec and a maximum value of 2.3 sec, indicating that the crustal velocities used to calculate synthetics are slightly faster than the actual values for most paths from this event. The moment tensor inversion using a similar crustal model for the northeastern United States (Yang and Aggarwal, 1981; Du *et al.*, 2003) produced almost identical results with time shifts of 0.8 sec.

The preferred focal mechanism (Fig. 2) is dominantly strike slip with near-vertical nodal planes. The best-fitting double-couple source parameters are strike = 251°, dip = 70°, rake = 165°, and seismic moment = 1.3 ($\pm$0.5) $\times$ 10^{15} N m. This nodal plane is consistent with the east-trending aftershock distribution discussed in the next section, which favors slip on the east-northeast–west-southwest (251°) nodal plane that dips steeply (70°) to the north. Be-

Table 1
2003 Bardwell, Kentucky, Earthquake and Other Significant Earthquakes in the Region

Date (yyyy/mm/dd)	Origin Time (hh:mm:sec)	Latitude (°N)	Longitude (°W)	Depth (km)	Magnitude* (m_b)	Magnitude* (M_w)	P axis (trend/plunge)	Reference†
				Bardwell Earthquake Solutions				
2003/06/06	12:29:34							
Catalog location		36.87	88.97	2.5	4.5		315/11	First motion
Centroid location		36.875	89.010	2.0	4.5	4.0	118/04	Waveform
		36.89	88.99	5		4.02	298/07	9
				New Madrid Seismic Zone				
1962/02/02	06:43:34	36.37	89.51	7.5	4.3	4.2	042/19	1
1963/03/03	17:30:11	36.64	90.05	15		4.6	259/28	6
1965/08/14	13:13:56	37.22	89.31	1.5	3.8	3.6	239/28	1,8
1970/11/17	02:13:55	35.86	89.95	16	4.4	4.1	272/09	1
1975/06/13	22:40:27	36.54	89.68	9	4.2	3.7	049/34	1
1976/03/25	00:41:20	35.59	90.48	16	5.0	4.6	272/01	1,8
1990/09/26	13:18:51	37.16	89.58	15	4.7	4.2	242/28	6
1991/05/04	01:18:55	36.56	89.83	8	4.6	4.1	042/03	6
1994/02/05	14:55:37	37.36	89.19	16	4.2	3.8	255/07	6
				Illinois Basin and Wabash Valley Seismic Zone				
1968/11/09	17:01:42	37.91	88.37	22	5.5	5.2	098/0	1,2,3,8
1974/04/03	23:05:03	38.55	88.07	15	4.7	4.4	267/14	1
1987/06/10	23:48:55	38.71	87.95	10	4.9	5.0	088/04	4,5,6
2002/06/18	17:37:17	37.992	87.772	18	5.0	4.6	252/10	6
				Ozark Uplift				
1965/10/21	02:04:38	37.48	90.94	5	4.9	4.6	272/75	1
1967/07/21	09:14:49	37.44	90.44	15	4.3	4.0	50/5	1,6

*Magnitude: m_b, mb (Lg); 1-sec period Lg-wave magnitude; M_w, moment magnitude.
†Reference: (1) Herrmann, 1979; (2) Stauder and Nuttli, 1970; (3) Gordon, 1988; (4) Taylor *et al.*, 1989; (5) Langer and Bollinger, 1991; (6) Herrmann and Ammon, 1997; (7) Kim, 2003; (8) Nuttli, 1982; (9) Herrmann (personal comm., 2004; www.eas.slu.edu/Earthquake_Center).

cause the P axis is nearly horizontal (plunge = 4°) and trends east-southeast–west-northwest (118°), right-lateral strike slip on an east-northeast–west-southwest trending fault is indicated. This is surprising because this sense of slip is inconsistent with estimates of the direction of the maximum compressive stress near the NMSZ of about 80° (Grana and Richardson, 1996), 73–84° (Ellis, 1994), or 75° (Zoback, 1992). A similar focal mechanism but with the east-northeast nodal plane dipping steeply south is obtained by Herrmann at St. Louis University (personal comm., 2003) (Table 1).

The preferred source depth is found by running the inversion for a range of source depths seeking the global minimum misfit. Figure 3 illustrates the changes in fitting error and source mechanism as a function of focal depth. The focal depth plotted is the depth used to generate the synthetics. For this earthquake, the fitting error reaches a minimum at 1 km depth although the focal mechanism and the fitting error for depths between 0.5 and 3 km do not vary significantly.

Aftershock Location

We deployed five broadband seismometers within 15 hr of the mainshock (Fig. 4). The early regional network location of the mainshock was very close to SUL, the first temporary station deployed. Other station locations were chosen to lie about 4 km from SUL at varying azimuths. The resulting network design was asymmetric with respect to the aftershock locations, but not sufficiently to warrant a significant reconfiguration. Station NEAL, installed on 18 June 2003, reduced the largest azimuthal gap. OPE was moved to site OPE2 on 19 June 2003 because of potential flooding. All stations were removed on 2 July 2003. Station locations are given in Table 2.

The three-component broadband seismometers have an instrument response that is flat to input ground velocity between 0.033 Hz and 50 Hz. At each site, seismic signals were recorded continuously at 100 samples per sec.

Over approximately four weeks, 253 seismic events were identified for the Bardwell aftershock dataset. These included local, regional, and teleseismic events and noise triggers. After event association, P- and S-wave arrival times were picked and HYPOELLIPSE (Lahr, 1999) was used to locate the events. We modified the NMSZ velocity model (Chiu *et al.*, 1992) to locate the earthquakes. This is the standard network model for locating earthquakes in the NMSZ. We decreased of the top layer thickness from 600 to 340 m. The adjustment to the soil-layer thickness was based on the soil thickness in three wells (KY18, 399 m; KY19, 249 m; KY8, 304 m) that penetrate to Paleozoic rocks in the area (Dart, 1992). The velocity model is given in Table 3.

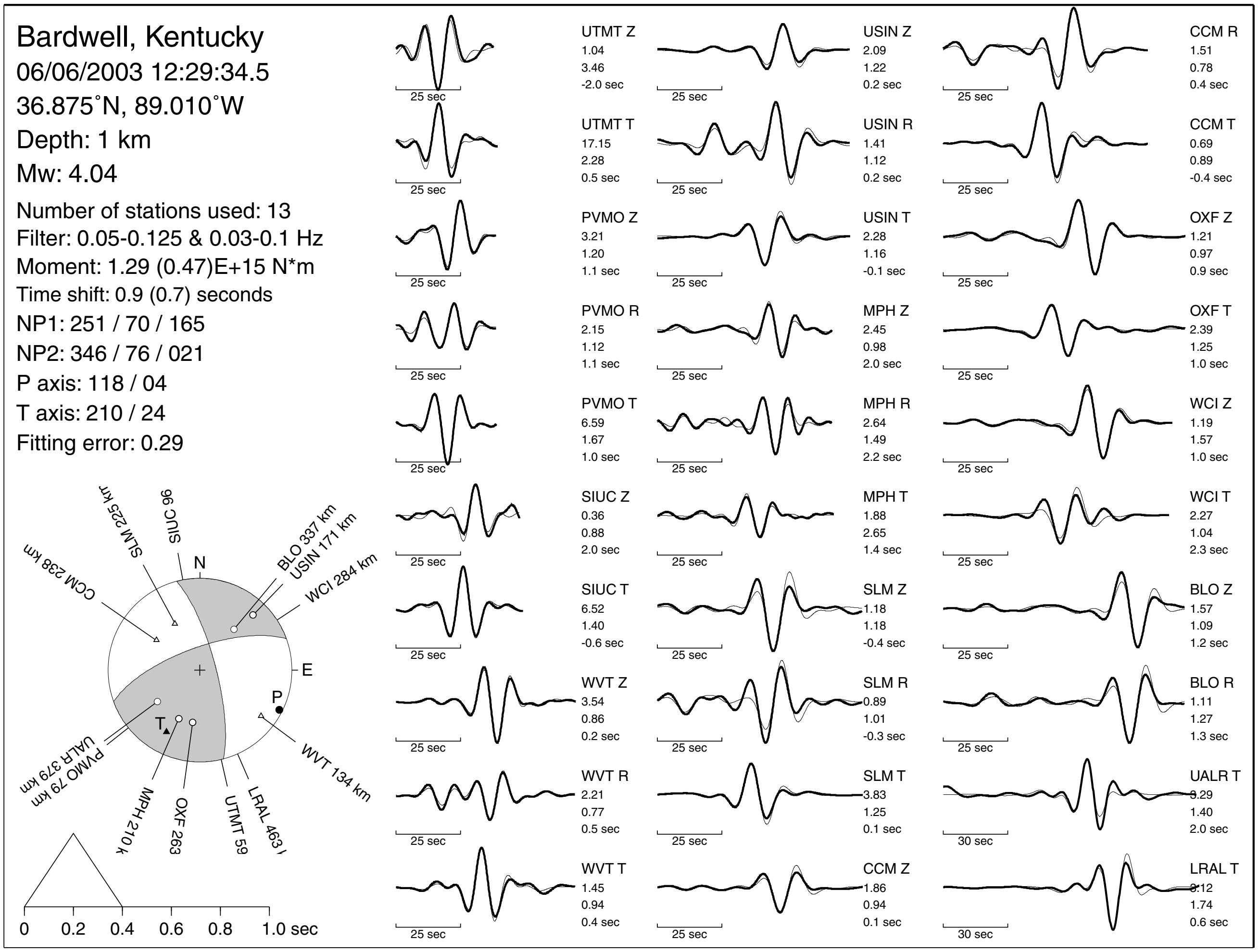

Figure 2. Comparison between observed (gray lines) and synthetic (black lines) waveforms of the 6 June 2003 earthquake. Synthetic seismograms are calculated for a focal depth of 1 km. Station code and component (Z, vertical; R, radial; T, transverse components), peak amplitude of the observed signal in micrometers, seismic moment in 10^{15} N m, and time shift δt in seconds are indicated at the end of each trace. The focal mechanism of the event is represented by the typical beach-ball representation of lower-hemisphere projection. Shaded quadrants denote compression for *P* waves. The epicentral distance of each station is marked around the beach ball according to azimuth. For those stations whose *P*-wave polarity data are used, a circle is plotted for compressional first motion and a triangle is used for dilatational first motion. Two nodal planes (NP1 and NP2) and the azimuth and plunge angle in degrees of the *P* and *T* axes are indicated. The simple triangular source-time function used is shown.

Of the 253 identified seismic events, 85 were local aftershocks with very good signal-to-noise ratios at all stations. Initial event locations were determined with no station corrections. We defined station corrections as the average of the residuals for each station (*P* and *S* waves independently) for the 85 events. The station corrections are given in Table 2. These station corrections were applied when relocating the 85 aftershocks.

The aftershock locations are shown in Figure 4a as open circles. They occur directly underneath the town of Bardwell. The aftershocks define a relatively narrow east–west trend roughly 1 km in length and 0.25 km in width. The distribution of these aftershocks in the north–south cross section (open circles) shown in Figure 4b indicates a nearly vertical rupture area between 1.5 and 3.0 km depth.

A goal of this study is to determine the fault geometry of the mainshock from the distribution of aftershocks. However, the level of uncertainty in aftershock location is on the order of the dimension of the fault plane (see Fig. 8b). The mean horizontal and vertical 68% confidence estimates are 0.4 and 1.0 km, respectively. Multiple realizations of an earthquake located at the same point and having this level of uncertainty should produce an ellipsoidal cloud with dimensions of the level of uncertainty. This suggests the actual

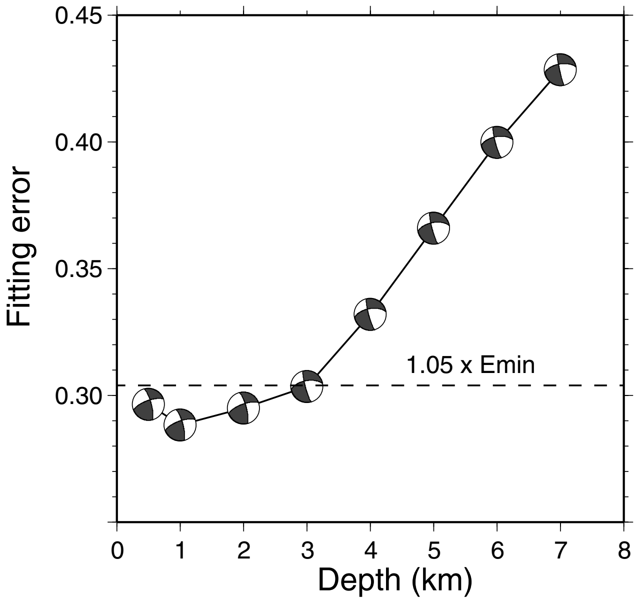

Figure 3. Changes of the fitting error (E) and source mechanism as a function of focal depths for the 6 June 2003 Bardwell, Kentucky, earthquake. The fitting error reaches a global minimum (E_{min}) at 1 km depth. The inversion results for focal depths between 0.5 and 3 km produce similar overall waveform fits and source mechanisms indicating a range of acceptable depths. Acceptable results fall below the horizontal dashed line representing 5% greater fitting error, $1.05 \times E_{\mathrm{min}}$.

level of uncertainty is overestimated for these events and that the locations are better than the level of uncertainty suggests.

This led us to try a high-resolution hypocenter location algorithm. We used the double-difference earthquake location method (Waldhauser and Ellsworth, 2000). The method incorporates travel-time differences formed from *P*- and *S*-wave arrival times with differential travel times derived from waveform cross-correlation methods. It is suggested that uncertainties are improved by an order of magnitude for two basic reasons (Waldhauser and Ellsworth, 2000). First, specifying the travel time as a double difference minimizes errors due to unmodeled velocity structure. In the Mississippi embayment with deep soils, this could prove significant. Second, waveform cross-correlation measurements are potentially more accurate than picks made by an analyst, in particular, for *S* waves where the onset is often obscured by the *P*-wave coda.

Although Waldhauser and Ellsworth (2000) used the cross-spectral method of Poupinet *et al.* (1984) to measure the differential travel times, we found it unstable for signals that are not quite similar. Hence, we chose to use a cross-correlation method that we find more stable for analysis of broadband waveforms. The cross-correlation method used in our study is illustrated in Figure 5. In this example, the *P* waves from two events at site SUL are correlated. The data are bandpass filtered between 0.6 and 30 Hz, and a 1.28-sec window is applied. The windows are centered on the same specified time relative to the origin time of each event (Fig. 5a). This specified time corresponds to the travel time of the phase in question for the first event. The cross-correlation of the two time series is shown in Figure 5b. The differential travel time corresponds to the lag time of the peak in the cross-correlation function. For use in the double-difference earthquake location, only measurements having a correlation coefficient equal to or larger than 0.8 are retained, and the correlation coefficient is used to weight the uncertainty of the observations. The method has a precision of one sample (0.01 sec in this study), and it is a stable estimator because nonsimilar signals do not satisfy the correlation coefficient threshold. Examples of correlated *P*, and *S* wave at two stations from the same event are shown in Figure 5c.

The relocations using the double-difference method are shown in the open rectangle inset in Figure 4. Epicenter locations have only modest changes, and the mean of the horizontal uncertainty has been reduced from 400 to 21 m. The distribution of epicenters still defines an east–west trend roughly 1 km in length. A substantial compressing of the vertical distribution of hypocenters is apparent in the transverse cross section shown in the open rectangle inset in Figure 4b, and the mean of the vertical uncertainty has been reduced from 1000 to 25 m. The hypocenters define a nearly vertical fault ranging from 2.0 to 2.7 km depth. An east–west cross–section (along strike) is shown in Figure 4c. The circular "fault plane" shown in this cross section contains 90% of the hypocenters and has a radius of 0.44 (± 0.03) km. The uncertainty in the radius is based on the mean uncertainty in the earthquake locations.

Aftershock Focal Mechanisms

Although the portable seismographic network we deployed has a limited number of stations, each station is a high-quality broadband seismograph recording three components of ground motion. This enables substantial processing of the waveform data to help obtain significantly more information at each site. For each trace, instrument response is removed, horizontal components are rotated to radial and transverse components, and all three components are integrated to displacement after applying a high-pass filter (corner = 0.4 Hz). After this processing, *SH*- and *SV*-wave polarities and the amplitude ratios of seismic phases can be determined, in addition to the *P*-wave first motions. Figure 6a shows waveforms at station SUL for the example earthquake (event 4). In this case, the *SV*-wave polarity is clearly observed on the radial component, and the *SH*-wave polarity is clearly observed on the transverse component. Although the signal-to-noise ratio was typically sufficient at station SUL to provide clear displacement waveforms, such clarity at other stations was less typical.

To determine the double-couple earthquake focal mechanism we utilized *P*, *SH*, and *SV* first-motion observations

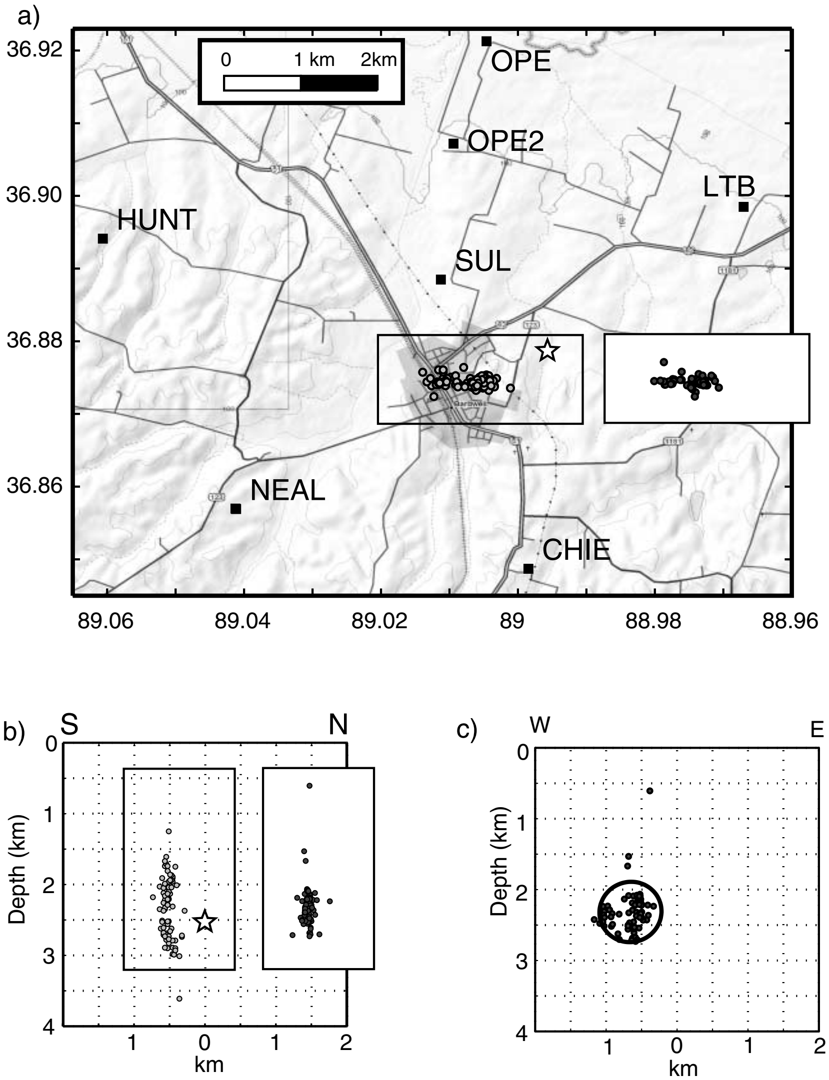

Figure 4. (a) Broadband seismometers (black squares) deployed following the Bardwell earthquake. The star indicates the mainshock epicenter. Initial aftershock epicenters (open circles in the unfilled rectangle) clearly delineate an east-trending zone approximately 1 km in length. Relocated epicenters are plotted as dark circles in the white-filled inset. Both rectangles are geographically the same area. (b) North–south cross section shows aftershocks are consistent with a vertical east-trending fault. The relocated hypocenters (dark circles in white-filled inset) are more concentrated in the vertical dimension, and they are still consistent with a vertical fault. (c) A circle of radius 0.44 km, including 90% of the relocated aftershocks, is displayed in this east–west cross section.

Table 2
Station Information for Bardwell Aftershock Network

Station Code	Latitude (°N)	Longitude (°W)	Elevation (m)	*P* correction (sec)	*S* correction (sec)
SUL	36.88848	89.01125	109	0.00	−0.05
LTB	36.89849	88.96704	102	0.00	0.16
HUNT	36.89412	89.06062	117	0.01	0.11
OPE	36.92128	89.00458	98	−0.01	0.07
OPE2	36.90718	89.00941	105	0.00	0.03
CHIE	36.84871	88.99847	136	0.00	−0.06
NEAL	36.85692	89.04115	132	0.01	0.06

Table 3
Modified New Madrid Velocity Model

Layer No.	Thickness (km)	V_P (km/sec)	V_S (km/sec)
1	0.34	1.80	0.60
2	2.16	6.02	3.56
3	2.5	4.83	3.20
4	12.0	6.17	3.57
5	10.0	6.60	3.82
6		7.30	4.22

and amplitude ratios *SV/SH*, *SH/P*, and *SV/P* to constrain the possible focal mechanisms (FOCMEC) (Snoke *et al.*, 1984; Snoke, 2003). Figure 6b shows the focal mechanism for the example event determined using the program FOCMEC and the larger set of constraints. The focal mechanisms obtained using only the *P*-wave first motions at each station (e.g., FPFIT) (Reasenberg and Oppenheimer, 1985) were unacceptable, because multiple focal mechanisms were formed to fit observed first motions.

Focal mechanisms determined for a subset of aftershocks are shown in Figure 7. Most of this subset of aftershocks occurred after installation of the station NEAL on 18 June (Table 4). Although the selection of earthquakes is somewhat arbitrary, the set still samples along the length of the fault. In general, focal mechanisms among these after-

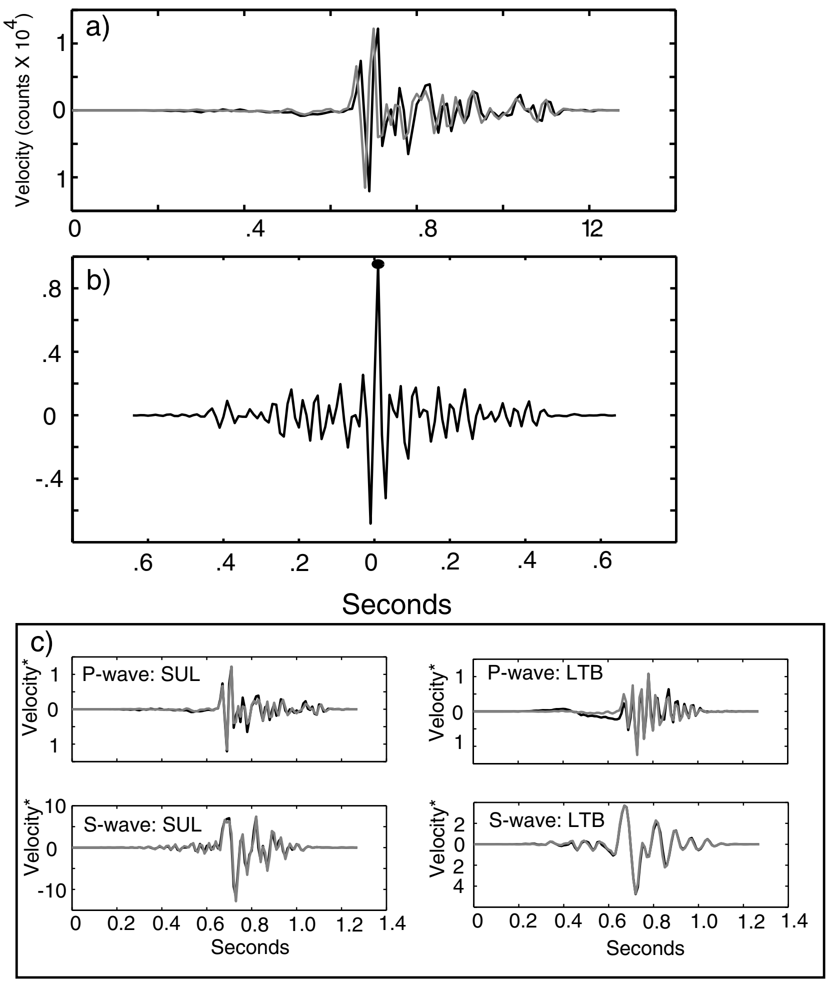

Figure 5. (a) *P*-wave window for two events plotted relative to the adjusted arrival time (see text). (b) Normalized cross-correlation showing optimum lag time, (differential travel time). (c) Examples of *P* and *S* waves at two stations after adjustment by lag time.

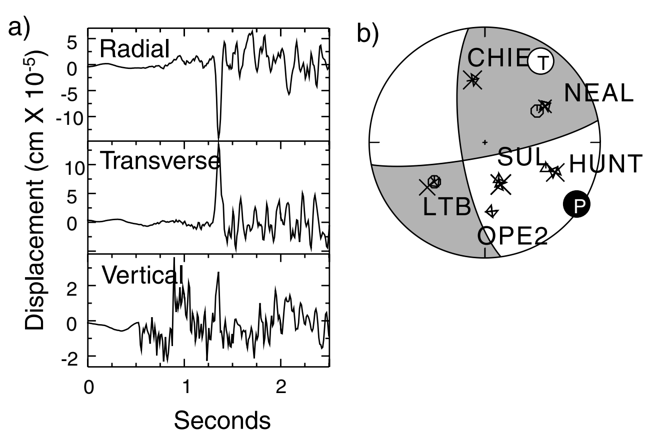

Figure 6. (a) Displacement waveforms at station SUL for event 4. Horizontal waveforms are rotated to radial and transverse allowing identification of *S*-wave polarity. (b) Focal mechanism for event 4.

shocks are consistent with right-lateral strike slip on a nearly vertical east-striking fault plane. The average *P* axis for these events is nearly horizontal and trends east-southeast (~120°), which is almost identical with the mainshock *P*-axis orientation shown in Figure 2.

Constraints on the Mainshock Location Using Waveform Cross-Correlation

The mainshock location plotted in Figure 4a as a star (Table 1) was derived from arrivals observed on the regional network and observations from the Kentucky seismographic network (Wang *et al.*, 2003). It does not fall within the limits of the aftershock trend, but lies approximately 1 km to the northeast. The closest station used to locate the mainshock was 13.2 km away, and four stations were within 20 km. However, *S*-wave arrivals were not estimated at those stations. The closest station having an *S*-wave arrival time was 61 km away. The distribution of seismic stations in azimuth was good. The larger of the two horizontal 68% confidence estimates is 1.2 km, and the vertical 68% confidence estimate is 1.3 km for the mainshock.

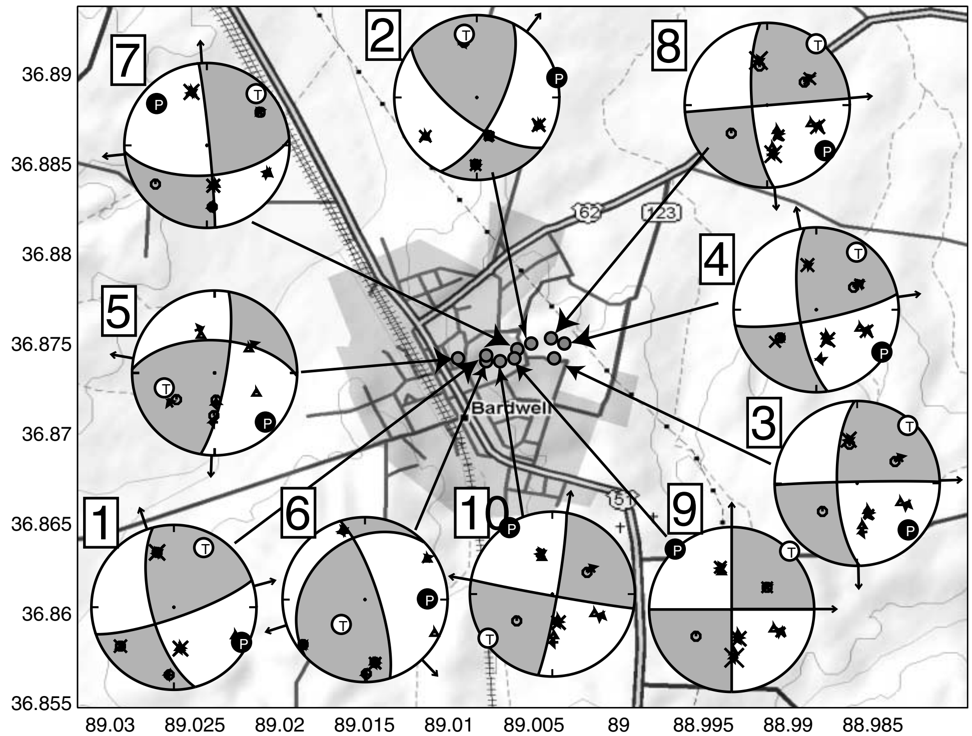

Figure 7. Aftershock focal mechanisms inferred from *P*- and *S*-wave polarities and ratios using the program FOCMEC. Event IDs are listed in Table 4.

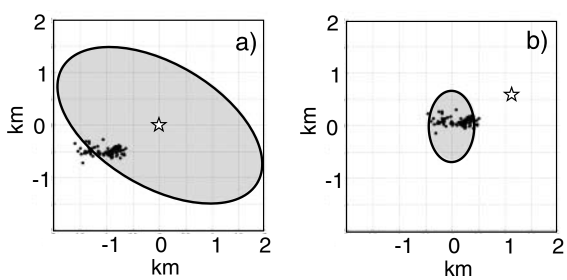

Figure 8. (a) Projection onto a horizontal plane of the 95% confidence ellipsoid for the mainshock location. Note that many aftershocks occur outside of the specified confidence area. (b) Projection onto a horizontal plane of the 95% confidence ellipsoid for an aftershock near the center of the distribution. Note that the mainshock location (star) is clearly outside the specified confidence area for this event.

Figure 8a shows a projection of the 95% confidence ellipsoid for the mainshock onto a horizontal plane centered on its epicenter. At this level of probability, more than half of the aftershocks are within the uncertainty ellipsoid for the mainshock. Figure 8b shows the projection of the 95% confidence ellipsoid for an aftershock near the center of the distribution (the aftershock uncertainty is from the original location using HYPOELLIPSE). At the same level of probability, the mainshock lies well outside the uncertainty ellipsoid for this event. Given the larger level of uncertainty associated with the mainshock than the aftershocks, it is likely that the true mainshock hypocenter lies within the distribution of aftershocks.

The largest aftershock on 8 June 2003 (10:51, *M* 2.4; Table 4) can be used to support this claim, because it was well recorded by stations of the portable network and by the regional stations that also recorded the mainshock. Figure 9 shows waveform matching for the vertical records at CCM (Cathedral Cave, Missouri, $\Delta = 238$ km) from the mainshock and the largest aftershock. Waveforms are cross-correlated with a coefficient of 0.64, suggesting that the two events are somewhat similar in their location and source radiation. Geller and Mueller (1980) and Nadeau *et al.* (1995) suggest using one quarter of the dominant signal wavelength as a measure location uncertainty for two well-correlated events. In this case, *Lg* waves have a velocity of 3.5 km/sec and a dominant frequency near 2 Hz giving a quarter wavelength of about 450 m. The waveform similarity suggests these two events are within 450 m (Geller and Mueller, 1980; Thorbjarnardottir and Pechmann, 1987). However, Harris (1991) reported that the correlation length can be much longer, one to two wavelengths in some regions. The centroid of the aftershock distribution at 36.875° N and 89.010° W and depth of 2.4 km is our preferred mainshock location.

Table 4
Mainshock and Large Aftershocks

Event ID	Date (mm/dd/yyyy)	Time (hh:mm:sec)	Latitude (°N)	Longitude (°W)	Depth (km)	Magnitude (M_L)
Main	06/06/2003	12:29:34.00	36.875	89.010	2.0	4.5
1	06/07/2003	11:07:00.18	36.8743	89.0085	2.08	1.9
	06/08/2003	01:02:14.70	36.8740	89.0040	1.70	2.0
2	06/08/2003	10:51:38.80	36.8750	89.0058	2.13	2.4
	06/09/2003	07:32:28.85	36.8748	89.0060	2.78	2.2
	06/10/2003	07:41:33.26	36.8743	89.0065	2.05	2.1
	06/12/2003	20:05:27.85	36.8743	89.0065	2.09	2.1
	06/12/2003	22:51:39.54	36.8750	89.0068	3.10	2.1
3	06/21/2003	07:47:51.61	36.87417	89.00450	2.53	1.6
4	06/23/2003	04:13:08.83	36.87483	89.00484	2.54	1.7
5	06/23/2003	06:15:23.63	36.87417	89.01017	2.52	1.3
6	06/24/2003	12:21:43.52	36.87400	89.00850	0.99	1.4
7	06/25/2003	01:21:02.63	36.87433	89.00750	2.18	1.5
8	06/27/2003	05:40:32.25	36.87500	89.00484	2.53	1.7
9	07/02/2003	10:36:31.50	36.87417	89.00684	2.76	1.9
10	07/02/2003	10:37:20.21	36.87400	89.00767	2.86	1.3

Events identified by IDs are those aftershocks used to determine focal mechanisms plotted in Figure 7. Event 2 is the largest aftershock, which was used as the master event to relocate the mainshock with regional waveform data.

Discussion

Relocation of the aftershocks using the double-difference earthquake location method (Waldhauser, 2001) significantly reduced the location uncertainty while leaving the east–west trend in epicenters largely unchanged. The distribution of aftershocks in a north–south cross section is consistent with a nearly vertical east-striking fault at depths between 2.0 and 2.7 km. For the east–west cross section (along strike), a circular "fault plane" containing 90% of the hypocenters has a radius of about 0.44 (± 0.03) km.

One of the main values of this aftershock deployment is that the constraints placed on the faulting geometry of the mainshock by the distribution of aftershocks allow inferences regarding source scaling. The fault radius can be used along with the seismic moment obtained from the waveform inversion to determine the static stress drop, $\Delta\sigma$, of the mainshock. The relationship between static stress drop, seismic moment (M_0), and fault radius (r) is given by $\Delta\sigma = (7/16) M_0/r^3$ (Keilis-Borok, 1959; Kanamori and Andersion, 1975). For the seismic moment, $M_0 = 1.3 \times 10^{15}$ N m, the mainshock has a static stress drop $\Delta\sigma = 67$ (± 14) bars, where the uncertainty is related entirely to the uncertainty in fault radius. Atkinson and Hanks (1995), based on fits to high-frequency ground-motion observations, suggest that the average stress drop for earthquakes in eastern North America is 150 bars. The variability between earthquakes is substantial, however, and 67 bars is not unusual.

Although earthquakes in the NMSZ generally concentrate in the Precambrian basement over the depth range of 4–14 km (Chiu *et al.* 1992; Pujol *et al.* 1997), the Bardwell aftershocks are concentrated between depths of 2.0 to 2.7 km consistent with estimates of the focal depth of the mainshock. The M_w 3.6 event of 14 August 1965 (Table 1 see Fig. 11) also has a shallow source depth of 1.5 km (Herrmann, 1979; Nuttli, 1982). These events nucleate and propagate entirely within Paleozoic sedimentary rocks, because the top of the Precambrian basement is between 3 and 4 km deep in this area (McBride *et al.*, 2003). Rupture that nucleates within the Paleozoic rocks indicates that these rocks store potential strain energy. A search of the Center for Earthquake Research and Information (CERI), University of Memphis catalog for events in the immediate area since 1992 produces:

- the m 2.1 Lovelaceville, Kentucky, with depth of 9.1 km (11 January 1993),
- the m 2.6 Blandville, Kentucky, with depth of 8.2 km (29 July 1993),
- the m 3.4 Blandville, Kentucky, with depth of 12.7 km (26 September 1994),

showing that earthquakes also occur over a normal depth range in the study area.

A discrepancy of about 20° exists between the east–west-trending distribution of aftershocks and the west-southwest–striking nodal plane (strike = 251°) of the mainshock focal mechanism (LDEO) obtained from waveform modeling. To obtain another independent estimate of the fault plane orientation, we computed P-wave first-motion focal mechanisms for the mainshock by using the program FOCMEC. Figure 10a shows the range of solutions that fit the first-motion observations with no discrepancies. Of these, the solution shown with the heavy black lines having strike = 90°, dip = 89°, and rake = −165° is best supported by the nearly vertical east-striking distribution of

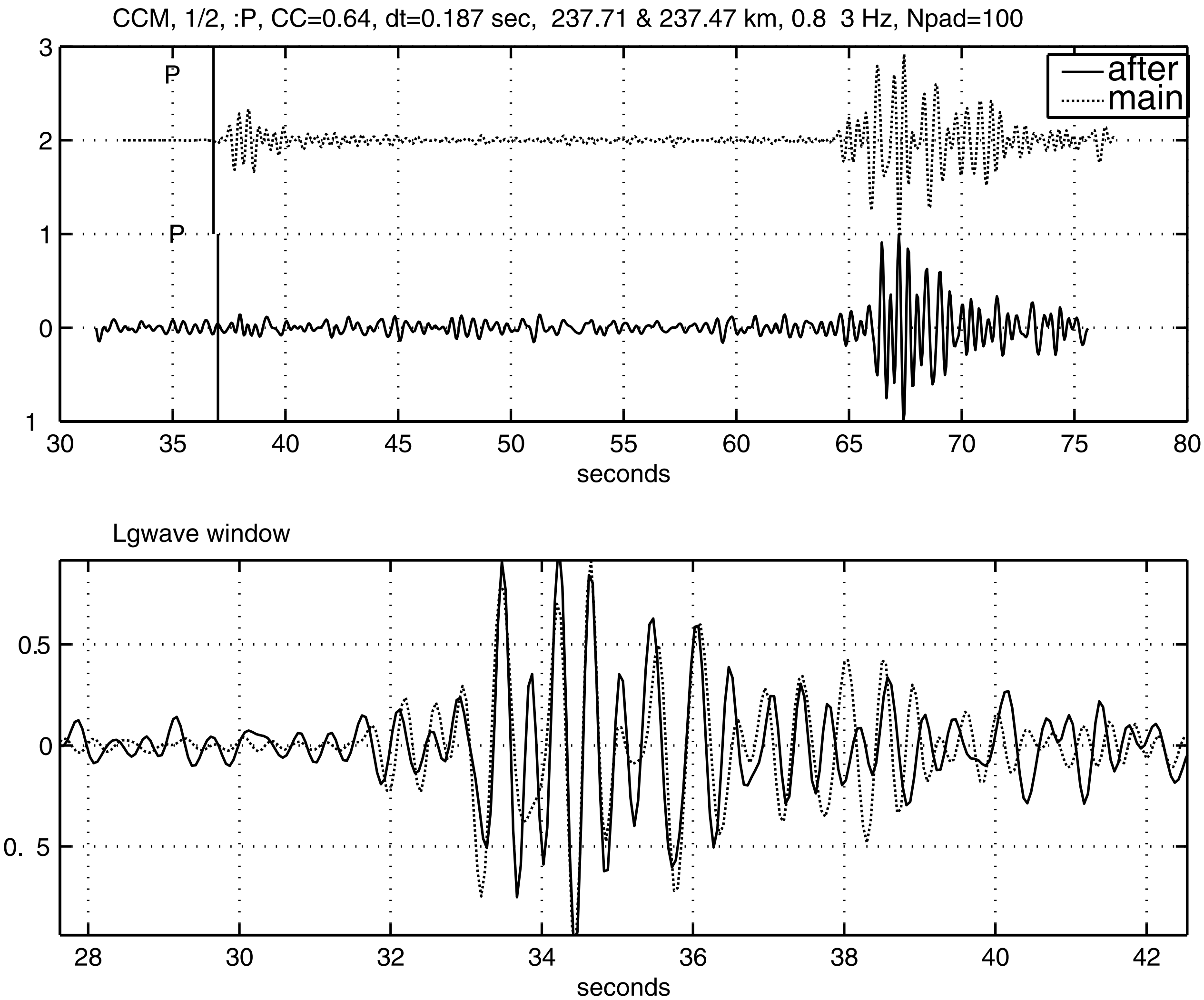

Figure 9. (upper panel) Regional east–west component records at CCM ($\Delta = 238$ km, AZ $= 304°$) from the mainshock (dotted trace) and the largest aftershock on 8 June 2003 10:51 (*M* 2.4) (solid trace). Traces are plotted aligned to their *P*-wave travel times (lower panel). Two traces are superposed after the waveform cross-correlation. Notice that cross-correlation is performed for 35 sec, and the waveforms appear to be correlated to their largest-amplitude arrivals (i.e., *Lg* arrivals) with correlation coefficient 0.64 and time lag of 0.187 sec, whereas the *P* waves are misaligned. Because of the poor signal-to-noise ratio of the *P* window for the aftershock, differential *S-P* times could not be determined, which could put constraint on the mainshock location relative to the master event.

aftershocks. Figure 10b shows two mainshock focal mechanisms derived from waveform modeling of regional data with the first-motion observations. Both the LDEO solution (solid lines) and the St. Louis University solution from Table 1 (dotted lines) have several misfits. Based on these results, we conclude that rupture occurred on an east–west-trending vertical fault.

These results also indicate a larger uncertainty (~20° in strike and dip) is associated with the LDEO focal mechanism than the formal estimated uncertainty in the strike, dip, and rake of 4°, 6°, and 7°, respectively (see Du *et al.*, 2003). These uncertainties may be due in part to the simple 1D crustal model used for all source-station paths, because the true propagation paths involve complex crustal structure across the Mississippi embayment and Illinois basin (see Fig. 1). For shallow earthquakes such as this, surface waves that dominate the waveforms may be more affected by these lateral variations than the deep diving body waves observed as first motions.

To assess the state of stress around the Bardwell area, we invert the focal mechanisms of the mainshock and aftershocks for the local stress tensor (Gephart, 1990). The results of the stress inversion indicate that the local σ_1 trends 104° with a plunge of 5° (Fig. 11). The intermediate stress axis

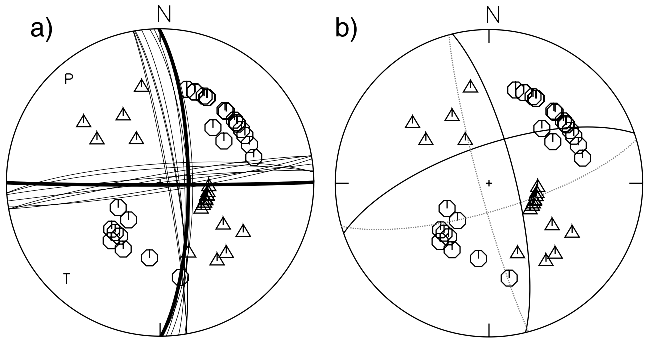

Figure 10. (a) The *P*-wave first-motion focal mechanism for the mainshock derived from regional network data. Multiple lines show the range of solutions that fit the first-motion observations with no discrepancies. The solution shown with heavy black lines has a nodal plane with strike = 90°, dip = 89°, and rake = −165°. This mechanism is favored by the nearly vertical east-striking distribution of aftershocks. (b) Shows two focal mechanisms derived from waveform modeling of regional data with the first-motion observations. Both the LDEO solution (solid lines) and the SLU solution from Table 1 (dotted lines) have a number of misfits.

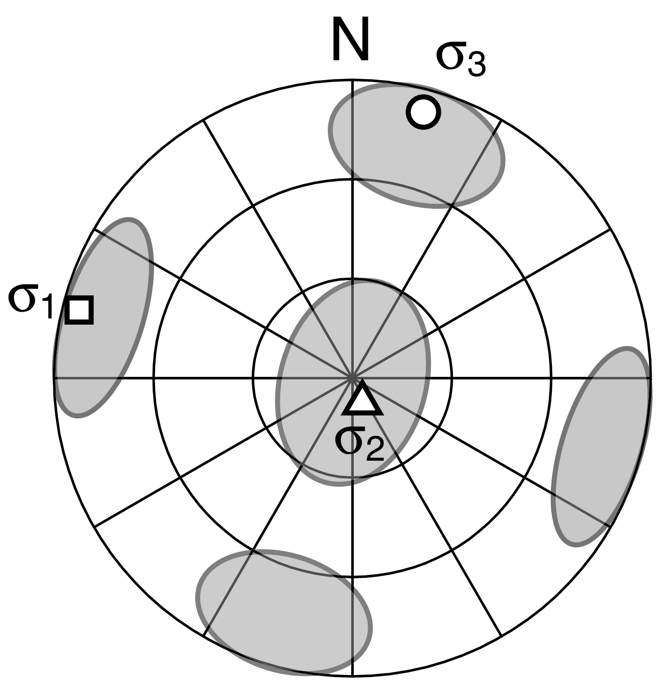

Figure 11. Maximum principal stress axis, σ_1 (square), intermediate axis, σ_2 (triangle), and least principal stress axis, σ_3 (circle), determined from inverting the focal mechanisms from ten aftershocks. The uncertainty in the axis orientation is shown as an ellipse. The σ_1 axis trends 104°.

(σ_2) is nearly vertical indicating a strike-slip stress regime (Gephart and Forsyth, 1984).

Zoback and Zoback (1991) find the direction of σ_1 measured throughout North America is remarkably consistent with the orientation of the plate-driving forces associated with the ridge-push force. For eastern North America as a whole, the mean σ_1 direction is estimated to be about 60–65°. The local stress field near Bardwell is therefore rotated around 40° clockwise relative to eastern North America. Others have observed a smaller σ_1 clockwise rotation for the NMSZ area to 80° (Grana and Richardson, 1996), 73–84° (Ellis, 1994), or 75° (Zoback, 1992). On an east-striking fault, these estimates would have produced left-lateral strike-slip motion rather than the right-lateral slip observed for the Bardwell sequence of earthquakes.

It is interesting to compare the focal mechanism of the Bardwell event to other similar size events in the region (Table 1, Fig. 12). Although most strike-slip earthquakes in the region have either northeast- or northwest-striking nodal planes, the four focal mechanisms with gray fill have north or east striking nodal planes. Oddly, the three with gray fill near New Madrid, Missouri, have the opposite sense of motion to the gray fill Bardwell mechanism. Because the σ_1 direction must lie in the quadrant containing the *P* axis (McKenzie, 1969), a rotation of the stress field is required where the σ_1 lies in the northeast quadrant for the New Madrid region but in the southeast quadrant near Bardwell. The implication is that a strong porturbation in the stress field occurs between Bardwell, Kentucky, and New Madrid, Missouri, a distance of about 60 km. Further, the stress field near New Madrid appears to deviate less with respect to that of eastern North America than the stress field near Bardwell.

Under the constraint that the σ_1 direction must lie in the quadrant containing the *P* axis, both the New Madrid and Bardwell gray fill mechanisms are generally compatible with the black fill while not being compatible with each other. An exception is the October 1965 earthquake in the Ozark Uplift that had a dip-slip focal mechanism. The rotation of stress field over a distance of 60 km between New Madrid and Bardwell may indicate a local source of stress in the crust. Potential sources of localized stress rotation in the NMSZ include static stress changes created by 1811–1812 earthquakes, local flexure due to sediment load, and buoyancy forces related to the "Rift pillow," although the latter would seemingly rotate the stress field for the red-fill earthquakes as well.

Conclusions

Regional and local waveform data from the 6 June 2003 Bardwell, Kentucky, earthquake sequence indicates that the M_w 4 mainshock occurred at a depth of about 2 (±1) km. The aftershocks delineate an east–west-trending, 1-km-long rupture area, and the hypocenters illuminate a nearly vertical plane between 2.0 and 2.7 km depth. The centroid of the

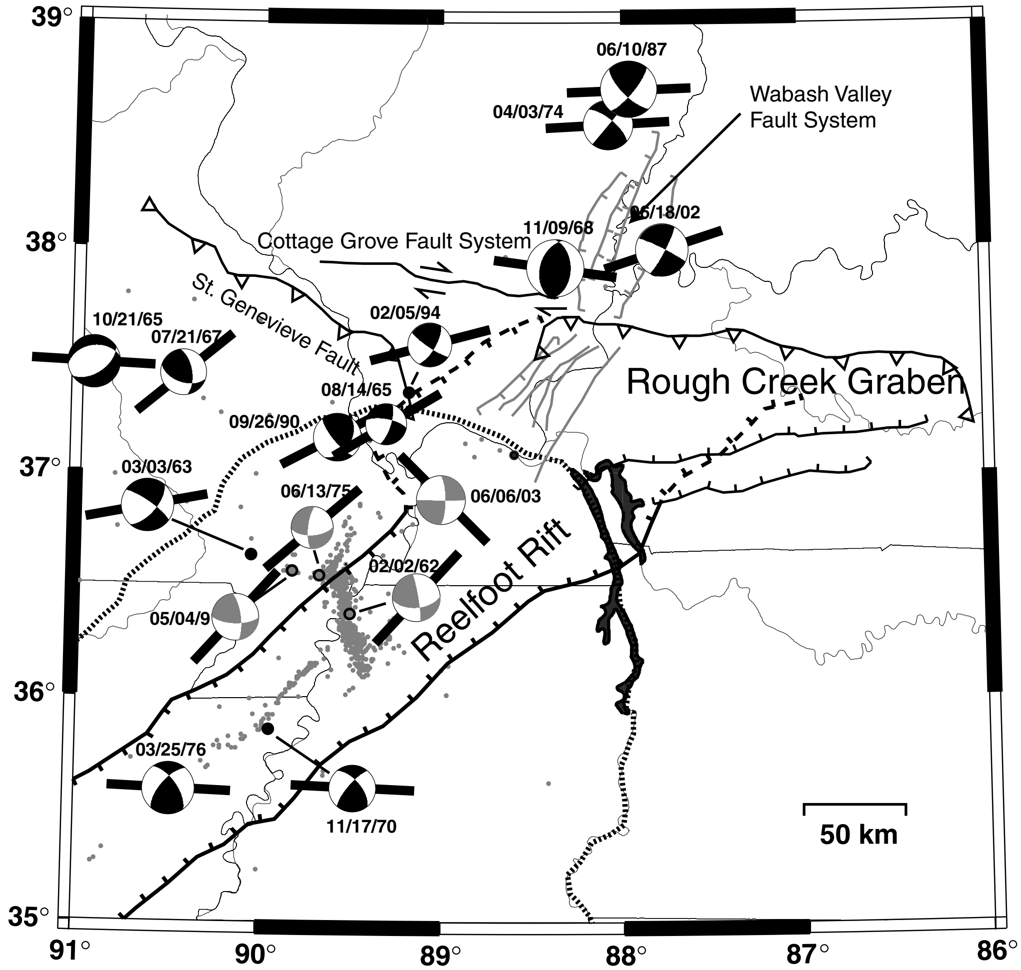

Figure 12. Focal mechanisms (lower hemisphere projection) of the earthquakes that have occurred in the central United States since 1960 are plotted, along with the orientation of the P axis (thick black line). Solid lines with teeth on the downthrown side show major geologic features around epicentral area. These are from the south; the Reelfoot rift, a failed rift system in the northern Mississippi embayment, Rough Creek graben in western Kentucky, and the Wabash Valley fault system (WVFS) along the southeastern Illinois-southwestern Indiana border. Tertiary limit that outlines the Mississippi embayment is indicated by heavy solid line. Earthquakes (gray circles) defining the New Madrid seismic zone (NMSZ) are shown to give the geometric orientation with the study area. The 6 June 2003 Bardwell, Kentucky, earthquake is indicated by a gray beach ball with a SW-trending P axis. Focal mechanisms of earthquakes near New Madrid with east–west-trending nodal planes that have northeast–east-northeast-trending P axes are plotted by gray beach balls with NE-trending P axes. A comparison between the Bardwell and New Madrid events indicates a strong perturbation in the stress field over a distance of about 60 km.

aftershock distribution is at 36.875° N, 89.010° W and depth of 2.4 km.

The source mechanism determined from regional waveform analysis shows predominantly strike-slip faulting with a west-southwest-striking nodal plane (dip $= 70°$ and strike $= 251°$) and a near horizontal P axis (plunge $= 4°$ and trend $= 118°$). However, a P-wave first-motion focal mechanism for the mainshock having strike $= 90°$, dip $= 89°$, and rake $= -165°$ is the best fit to the nearly vertical east-striking distribution of aftershocks. Rupture occurred on an east-west-trending vertical fault.

The aftershock cluster is interpreted as a circular fault area with a radius of about 0.44 (± 0.03) km. This source radius yields a static stress drop, $\Delta\sigma = 67$ (± 14) bars for the mainshock.

The local stress field near Bardwell is rotated about 40° clockwise relative to eastern North America as a whole. The Bardwell earthquakes have the opposite sense of slip to earthquakes that occur near New Madrid, Missouri. This requires a large rotation of stress field over a distance of 60 km providing evidence for a local source of stress in the crust.

Acknowledgments

We to thank John Filipcic at CERI, University of Memphis, for assisting with the aftershock survey. We are grateful to Russ Wheeler, Martin Chapman, Arch Johnston, Paul Richards and Jim Gaherty for their critical reviews and valuable comments. Zenming Wang at the Kentucky Geological Survey kindly provided waveform data from the Kentucky Network stations. This research work is supported by U.S. Geological Survey Grant 01-HQ-AG-0137 (to P.I., W.Y.K., LDEO). This is CERI contribution no. 479 and Lamont-Doherty Earth Observatory contribution no. 6665.

References

Atkinson, G. M., and T. C. Hanks (1995). A high-frequency magnitude scale, *Bull. Seism. Soc. Am.* **85,** 825–833.

Bertagne, A. J., and T. C. Leising (1991). Interpretation of seismic data from the Rough Creek graben of western Kentucky and southern Illinois, in *Interior Cratonic Basins: American Association of Petroleum Geologists Memoir 51*, M. W. Leighton, D. R. Kolata, D. F. Oltz, and J. J Eidel (Editors), *AAPG*.

Bickford, M. E., W. R. Van Schums, and I. Zietz (1986). Proterozoic history of the midcontinent region of North America, *Geology* **14,** 492–496.

Burke, K., and J. F. Dewey (1973). Plume-generated triple junctions; key indicators in applying plate tectonics to old rocks, *J. Geol.* **81,** 406–433.

Chiu, J. M., A. C. Johnston, and Y. T. Yang (1992). Imaging the active faults of the central New Madrid seismic zone using PANDA array data, *Seism. Res. Lett.* **63,** 375–393.

Dart, R. L. (1992). Catalog of pre-Cretaceous geologic drill-hole data from the upper Mississippi embayment: a revision and update of open-file report 90-260, *U.S. Geol. Surv. Open-File Rept. 92-685*.

Du, W.-X., W.-Y. Kim, and L. R. Sykes (2003). Earthquake source parameters and state of stress for northeastern United States and southeastern Canada from analysis of regional seismograms, *Bull. Seism. Soc. Am.* **93,** 1633–1648.

Ellis, W. L. (1994). Summary and discussion of crustal stress data in the region of the New Madrid seismic zone, *U.S. Geol. Surv. Open-File Rept. 1538-B*.

Ervin, C. P., and L. D. McGinnis (1975). Reelfoot rift: reactivated precursor to the Mississippi embayment, *Geol. Soc. Am. Bull.* **86,** 1287–1295.

Geller, R. J., and C. S. Mueller (1980). Four similar earthquakes in central California, *Geophys. Res. Lett.* **7,** 821–824.

Gephart, J. W. (1990). FMSI: a FORTRAN program for inverting fault/slikenside and earthquake focal mechanism data to obtain the regional stress tensor, *Comput. Geosci.* **16,** 953–989.

Gephart, J. W., and D. W. Forsyth (1984). An improved method for determining the regional stress tensor using earthquake focal mechanism data: application to the San Fernando earthquake sequence, *J. Geophys. Res.* **89,** 9305–9320.

Ginzburg, A., W. D. Mooney, A. W. Walter, W. J. Lutter, and J. H. Healy (1983). Deep structure of the northern Mississippi embayment, *AAPG Bull.* **67,** 2031–2046.

Gordon, D. (1988). Revised instrumental hypocenters and correlation of earthquake locations and tectonics in the central United States, *U.S. Geol. Sur. Profess. Pap. 1364*, 69 pp.

Grana, J. P., and R. Richardson (1996). Tectonic stress within the New Madrid seismic zone, *J. Geophys. Res.* **101,** no. B3, 5445–5458.

Harris, D. B. (1991). A waveform correlation method for identifying quarry explosions, *Bull. Seism. Soc. Am.* **81,** 2395–2418.

Herrmann, R. B. (1979). Surface wave focal mechanisms for eastern North America with tectonic implications, *J. Geophys. Res.* **84,** 3543–3552.

Herrmann, R. B., and C. J. Ammon (1997). Faulting parameters of earthquakes in the New Madrid, Missouri, region, *Eng. Geol.* **46,** 299–311.

Hildenbrand, T. G. (1985). Rift structure of the northern Mississippi embayment from the analysis of gravity and magnetic data, *J. Geophys. Res.* **90,** 12,607–12,622.

Hildenbrand, T. G., M. F. Kane, and J. D. Hendricks (1982). Magnetic basement in the upper Mississippi embayment region-a preliminary report, in *Investigations of the New Madrid, Missouri, Earthquake Region*, F. A. McKeown and L. C. Pakiser (Editors), *U.S. Geol. Surv. Profess. Pap. 1236*, 39–53.

Hildenbrand, T. G., M. F. Kane, and W. Stauder (1977). Magnetic and gravity anomalies in the northern Mississippi embayment and their spatial relation to seismicity, U.S. Geol. Surv. Misc. Field Studies Map MF-914, scale 1:1,000,000.

Howe, J. R. (1984). Tectonics, sedimentation and hydrocarbon potential of the Reelfoot aulacogen, *M.S. Thesis*, University of Oklahoma, Norman, 75 pp.

Kanamori, H., and D. L. Andersion (1975). Theoretical basis of some empirical relations in seismology, *Bull. Seism. Soc. Am.* **65,** 1073–1095.

Kane, M. F., T. G. Hildenbrand, and J. D. Hendricks, (1981). Model for the tectonic evolution of the Mississippi embayment and its contemporary seismicity, *Geology* **9,** 563–568.

Keilis-Borok, V. (1959). On estimation of the displacement in an earthquake source and of source dimension, *Ann. Geophys.* **12,** 205–214.

Kim, W.-Y. (2003). 18 June 2002 Caborn, Indiana Earthquake: reactivation of Ancient Rift in the Wabash Valley Seismic Zone? *Bull. Seism. Soc. Am.* **93,** 2201–2211.

Kolata, D. R., and T. G. Hildenbrand (1997). Structural underpinnings and neotectonics of the Southern Illinois Basin: an overview, in *Investigations of the Illinois Basin Earthquake Region*, T. G. Hildenbrand and D. R. Kolata (Editors), *Seism. Res. Lett.*, **68,** no. 4, 499–510.

Kolata, D. R., and W. J. Nelson (1991). Tectonic history of the Illinois Basin, *Am. Assoc. Petrol. Memoir* **51,** 263–285.

Kolata, D. R., J. D. Treworgy, and J. M. Masters (1981). Structural framework of the Mississippi embayment of southern Illinois, Illinois State Geol. Surv. Circular 516, 38 pp.

Lahr, J. C. (1999). HYPOELLIPSE: A computer program for determining local earthquake hypocentral parameters, magnitude, and first-motion pattern, *U.S. Geol. Surv. Open-File Rept. 99-23*.

Langer, C. J., and G. A. Bollinger (1991). The southeastern Illinois earthquake of 10 June 1987: the later aftershocks, *Bull. Seism. Soc. Am.* **81,** 423–445.

Langston, C. A. (1994). An integrated study of crustal structure and regional wave propagation for southern Missouri, *Bull. Seism. Soc. Am.* **84,** 105–118.

McBride, J. H., D. R. Kolata, and T. G. Hildenbrand (2003). Geophysical constraints on understanding the origin of the Illinois basin and its underlying crust, *Tectonophysics* **363,** 45–78.

McKenzie, D. P. (1969). The relation between fault plane solutions for earthquakes and the directions of the principal stresses, *Bull. Seism. Soc. Am.* **59,** 591–601.

Mooney, W. D., M. C. Andrews, A. Ginzburg, D. A. Peters, and R. M. Hamilton (1983). Crustal structure of the northen Mississippi embayment and comparison with other continental rift zones, *Tectonophysics* **94,** 327–348.

Munson, P. J., S. F. Obermeier, C. A. Munson, and E. R. Hajic (1997). Liquefaction evidence for Holocene and latest Pleistocene seismicity in the southern halves of Indiana and Illinois: a preliminary overview, *Seism. Res. Lett.* **68,** 521–536.

Nadeau, R. M., W. Foxall, and T. V. McEvilly (1995). Clustering and periodic recurrence of microearthquakes on the San Andreas fault at Parkfield, California, *Science* **267,** 503–507.

Newman, A., S. Stein, J. Weber, J. Engeln, A. Mao, and T. Dixon (1999).

Slow deformation and lower seismic hazard at the New Madrid seismic zone, *Science* **284,** 619–621.

Nuttli, O. W. (1982), Damaging earthquakes of the Central Mississippi Valley, *U.S. Geol. Surv. Profess. Pap. 1236-B*, 15–20.

Poupinet, G., W. L. Ellsworth, and J. Frechet (1984). Monitoring velocity variations in the crust using earthquake doublets: an application to the Calaveras fault, California, *J. Geophys. Res.* **89,** no. B7, 5719–5731.

Pujol, J., A. C. Johnston, J. M. Chiu, and Y. T. Yang (1997). Refinement of thrust faulting models for the central New Madrid seismic zone, *Eng. Geol.* **46,** 281–298.

Reasenberg, P. A., and D. Oppenheimer (1985). FPFIT, FPPLOT and FPPAGE: Fortran computer programs for calculating and displaying earthquake fault-plane solutions, *U.S. Geol. Surv. Open-File Rept. 85-739*.

Saikia, C. K. (1994). Modified frequency-wavenumber algorithm for regional seismograms using Filon's quadrature: modeling of Lg waves in eastern North America, *Geophys. J. Int.* **118,** 142–158.

Santillan, V. M., R. Smalley, Jr., and M. Ellis (2002). Deformation in the New Madrid Seismic Zone from continuous GPS Geodesy, AGU meeting at San Francisco, California.

Snoke, J. A. (2003). FOCMEC: Focal mechanism determinations, www.geol.vt.edu/outreach/vtso/focmec/.

Snoke, J. A., J. W. Munsey, A. C. Teague, and G. A. Bollinger (1984). A program for focal mechanism determination by combined use of polarity of SV-P amplitude ratio data, *Earthquake Notes* **55,** no. 3, 15.

Stauder, W., and O. W. Nuttli (1970), Seismic studies: South central Illinois earthquake of November 8, 1968, *Bull. Seism. Soc. Am.* **60,** 979–981.

Stearns, R. (1957). Cretaceous, Paleocene, and lower Eocene geologic history of the northern Mississippi embayment, *Bull. Geol. Soc. Am.* **68,** 1077–1100.

Taylor, K. B., R. B. Herrmann, M. W. Hamburger, G. L. Pavlis, A. Johnston, C. J. Langer, and C. Lam (1989). The southeastern Illinois earthquake of 10 June 1987, *Seism. Res. Lett.* **60,** 101–110.

Thorbjarnardottir, B. S., and J. Pechmann (1987). Constraint on relative earthquake locations from cross-correlation of waveforms, *Bull. Seism. Soc. Am.* **77,** 1626–1634.

Tio, H. K., and H. Kanamori (1995). Moment tensor inversion for local earthquakes using surface waves recorded at TERRAscope, *Bull. Seism. Soc. Am.* **85,** 1021–1038.

Tuttle, M. P., E. S. Schweig, J. D. Sims, R. H. Lafferty, L. W. Wolf, and M. L. Haynes (2002). The earthquake potential of the New Madrid seismic zone, *Bull. Seism. Soc. Am.* **92,** 2080–2089.

Waldhauser, F. (2001). HypoDD: a program to compute double-difference hypocenter locations, *U.S. Geol. Surv. Open-File Rept. 01-113*.

Waldhauser, F., and W. L. Ellsworth (2000). A double-difference earthquake location algorithm: method and application to the northern Hayward fault, California, *Bull. Seism. Soc. Am.* **90,** no. 6, 1353–1368.

Wang, Z., E. W. Woolery, and B. Shi (2003). Observed seismicity (earthquake activity) in the Jackson Purchase region of western Kentucky: January through June 2003, Special Publication 6, Kentucky Geological Survey, Series XII.

Wheeler, R. L., S. Rhea, S. F. Diehl, J. A. Drahovzal, G. W. Bear, and M. L. Sargent (1997). Seismotectonic map showing faults, igneous rocks, and geophysical and neotectonic features in the vicinity of the lower Wabash Valley, Illinois, Indiana, and Kentucky, *U.S. Geol. Surv., Geological Investigation Series, I-2583-D*, 19 pp.

Yang, J., and Y. P. Aggarwal (1981). Seismotectonics of northeastern United States and adjacent Canada, *J. Geophys. Res.* **86,** 4981–4998.

Zhao, L. S., and D. V. Helmberger (1994). Source estimation from broadband regional seismograms, *Bull. Seism. Soc. Am.* **84,** 91–104.

Zoback, M. D., and M. L. Zoback (1991). Tectonic stress field of North America and relative plate motions, in *Neotectonics of North America*, D. L. Slemmons, E. R. Engdahl, M. D. Zoback, and M. D. Blackwell (Editors), Geological Society of America, Boulder, Colorado, 339–366.

Zoback, M. L. (1992). Stress field constraints on intraplate seismicity in Eastern North America, *J. Geophys. Res.* **97,** no. B8, 11,761–11,782.

Center for Earthquake Research and Information
University of Memphis
3876 Central Avenue
Memphis, Tennessee 38152
shorton@memphis.edu
(S.H., M.W.)

Lamont-Doherty Earth Observatory of Columbia University
61 Route 9W
Palisades, New York 10964
wykim@ldeo.columbia.edu
(W.-Y.K.)

Manuscript received 17 March 2004.